Numerical and experimental studies on a hybrid panel element for heating, cooling and ventilation

Lars Schinke [a], André Schlott [b], Maximilian Beyer [a], Joachim Seifert [a]

[a] Chair of Building Energy Systems and Heat Supply, Institute of Power Engineering, Technische Universität Dresden, Dresden, Germany, lars.schinke@tu-dresden.de.

[b] Fraunhofer Institute for Manufacturing Technology and Advanced Materials IFAM, Branch Lab Dresden, Dresden, Germany, andre.schlott@ifam-dd.fraunhofer.de.

Abstract. The use of surface heating systems will become even more important in the future. On the one hand, the systems can be operated at lower system temperatures and thus represent an energy optimisation. On the other hand, such a system is very well recognised by the user in terms of thermal comfort. In addition, due to the hermetic construction of the buildings, a ventilation system is needed to ensure the necessary supply of fresh air. Considering the Covid-19 pandemic and the reduction of the risk of infection, the importance of fresh air supply is even higher. To meet these requirements, a hybrid panel element was designed and prototyped. The area of application includes new construction as well as the modernisation of residential and commercial buildings. The hybrid panel element combines the advantages of surface heating in winter with cooling in summer and all-season ventilation. The prototypes were used to carry out extensive measurement tests. This made it possible to prove the functionality of the hybrid surface system and to make statements regarding the performance parameters (transferable heat flux via the surface to the room and transferable heat flow to the air). In addition, a parameter study on influencing variables (e.g. material selection, arrangement of air channels) was carried out by means of numerical simulation.

Keywords. hybrid panel element, heating, cooling, ventilation, open-cell porous metals, numerical simulation, temperature distribution
DOI: https://doi.org/10.34641/clima.2022.410

1. Introduction

Radiant heating and cooling are well known in residential and non-residential buildings and will become even more important in the future. The good thermal comfort means that such a system is accepted by the users. Additionally, such systems represent an energy optimization by using lower system temperatures to operate. Recent buildings are more and more hermetic which introduces the need of a ventilation system to ensure the necessary supply of fresh air. This is even more important considering the current Covid-19 pandemic and the need to reduce infection risks. Up to now, the heating and ventilation of rooms have mainly been considered separately in terms of construction. For example, to simplify installation and media routing during building refurbishment, hybridising the room climate tasks of heating, cooling and ventilation in one component can be a clear advantage. The focus of the presented study is a modular element that fulfils the functions of surface heating or surface cooling and ventilation. Several research projects have already been carried out on this hybrid approach in the past, some of which also took thermal comfort into account in addition to functional and energy-related aspects. Investigations related to the application on the floor is available in [1]. For use on the ceiling, results can be found in [2-4]. The approach presented in this article is a single component/element that is used as surface heating/cooling as well as for conditioning the room supply air (therefore called hybrid panel element). This is to be used primarily on the ceiling. In the following, the various analyses (measurements and simulation) of this hybrid element are presented. A significant difference to systems available on the market is the use of open-cell porous metals in the hybrid element.

2. Description of the hybrid panel element

The element has a compact design consisting of a

water-carrying pipe system, which can deliver heat to the room (heating mode) and is able to absorb heat (cooling mode). At the same time, air is conditioned regarding its temperature before it is supplied to the room. As a special feature, cellular metallic materials (metal foam or metal fibre structures) are used in the element to improve the thermal properties and to realise a lightweight construction. This gives the element the following advantageous properties:

- fulfilment of all HVAC tasks incl. cooling
- lightweight and compact design
- very good heat distribution and, therefore, reduction of thermal inertia compared to classic underfloor heating
- thus, possibility to increase pipe distance at a nearly constant mean surface temperature
- very low surface temperature ripple
- variable installation options (ceiling or wall)

In recent years, extensive research on open-cell porous metals (OCPM) has taken place in materials science. Examples are the metal foam and the metal fibres, described in [5, 6]. These materials have various advantages for use in building energy technology, as shown in [7, 8]. The metal foam and the metal fibres were considered more closely as OCPMs and incorporated into the hybrid element. Both OCPM have different advantages for the intended use. A comprehensive thermal analysis of a composite of OCPM and a pipe is documented in [9].

In the first step, the dimensions of the hybrid element were based on the grid size 625 mm x 625 mm, which is common in grid ceiling construction. To have the greatest possible variety during the examinations, four channels were provided for the airflow in the element. These can be switched off separately depending on requirements. Fig. 1 shows an example of a hybrid element.

Fig. 1 – Example of a hybrid element

Various preliminary investigations have shown that the integration of the individual components (pipe, OCPM, air channel) especially poses some challenges from a manufacturing point of view. At this point, for example, the manufacturing tolerances of the individual components as well as the connection of the components (bonding, pressing) should be mentioned. For this reason, eight different demonstrators were manufactured. These differ in terms of the OCPM (metal foam (MFO)/metal fibre (MFI)/no OCPM), the position and material (copper/ polyethylene (PE)) of the tube in the OCPM and the manufacturing quality. Tab. 1 summarises the demonstrators investigated.

Tab. 1 – Properties of the built demonstrators

No.	OCPM	position of tube related to OCPM	tube material	manufacturing accuracy
V01	MFO	on	copper	low
V02	MFO	in	copper	low
V03	-	-	copper	low
V04	MFI	on	copper	low
V05	MFI	in	copper	low
V06	-	-	PE	high
V07	-	-	copper	high
V08	MFI	on	copper	high

3. Thermal investigations

The thermal investigation was divided into an experimental and a numerical simulations part. With the help of the experimental investigations, the various demonstrators had been analysed by measurement. Influences such as manufacturing tolerances and pipe material are shown by means of numerical simulations.

3.1 Experimental investigation

A test stand was designed and built for the experimental investigations (see Fig. 2).

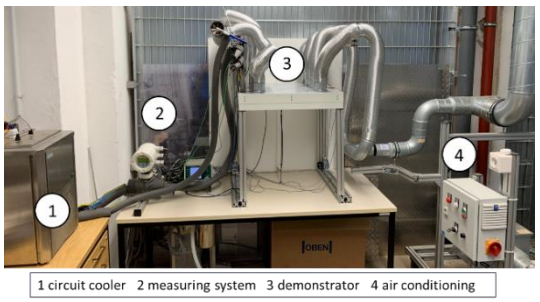

Fig. 2 – Test stand for experimental investigation

The water flowing through the pipes of the demonstrator (3) is tempered and the water volume flow is controlled with a circuit cooler (1). The air volume flow, which is guided through the air channels of the demonstrator (3), is realised by means of an air conditioning unit (4) consisting of a heater and a fan. With the aid of the measuring system (2), the water flow parameters (inlet and outlet temperature $\vartheta_{W,i}$ and $\vartheta_{W,o}$, water volume flow $\dot{V}_W$), air flow parameters (inlet and outlet temperature $\vartheta_{air,i}$ and $\vartheta_{air,o}$ per air channel and the total air volume flow $\dot{V}_{air}$) as well as the specific heat flux density on the room-facing side of the demonstrator are acquired. To be able to achieve meaningful results, the influencing parameters air volume flow, water volume flow and water inlet temperature are varied within a suitable range.

For the evaluation of the experiments, thermography

is used to analyse the surface temperature distribution on the room-facing side of the demonstrator. The caloric balances are drawn up for the media water and air in order to determine the respective heat fluxes. Furthermore, the specific heat flux from the element to the air on the room-facing surface is determined with heat flux measuring plates.

3.2 Numerical simulation

A 3D simulation was done using COMSOL Multiphysics. The model included the thermal modelling of all solid materials and the fluid flow of the air through the four channels. The geometric model was derived from the construction data of the demonstrators, which is shown in Fig. 3. The design represents the ideal thermal contact and neglects necessary manufacturing tolerances in most parts. This ideal case, which ignores the thermal resistances that occur in practice, serves to determine the target size for further optimisation.

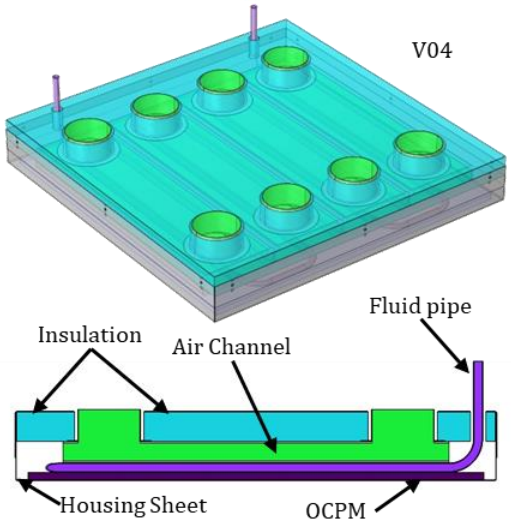

Fig. 3 – Geometric simulation model in transparent 3D (top) and 2D slice (bottom)

Special attention was paid to the connection between the fluid pipe and the OCPM. Since manufacturing tolerances lead to enormous thermal contact resistances, these tolerances were modelled to investigate their influence. Therefore, the tolerance range between the pipe and the air channel was filled in constructively and made accessible to the simulation (Fig. 4). The effect of these tolerances was approximated by varying the material data. Air is defined and examined as the worst case and aluminium as the ideal contact.

The boundary conditions were adapted so that they largely correspond to the experimental conditions. To include the convective heat transfer the basic characteristic [10] is used. The flow inside the air channels is also considered. The flow rate was varied between $\dot{V}_{air} = 0…75\ \mathrm{m^3/h}$. This corresponds to the experimental possibilities. To extrapolate higher volume flows, an air volume flow of $\dot{V}_{air} = 150\ \mathrm{m^3/h}$ was also simulated. The fluid flow inside the pipe was also set to $\dot{V}_W = 0.5\ \mathrm{L/min}$ according to the experimental conditions and kept constant for all variations.

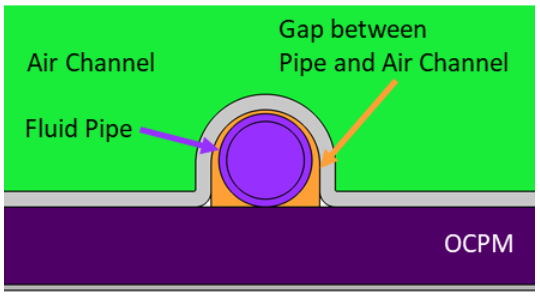

Fig. 4 – Detail of the filled tolerance space between heat transfer tube and air channel

The simulations were conducted with the element variants V03, V04 and V05 (see Tab. 1). The geometric differences are shown in Fig. 5 below.

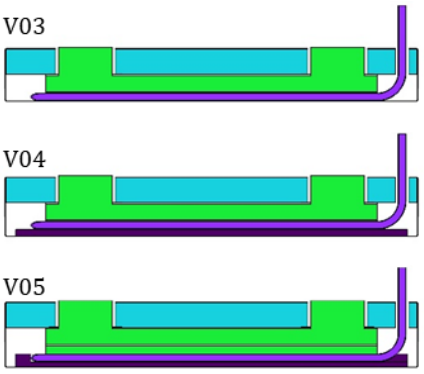

Fig. 5 – Simulated element variants

In element V03, there is no OCPM present and therefore this variant is the reference case. In elements V04 and V05 the fluid pipe is located on the OCPM or inside the OCPM, respectively. As an extension to the experimental investigations, the air channels used for air flow were varied. As shown in Fig. 3, there are 4 channels within the model. When all 4 channels are used the variants are labelled 4C. Variants then only use the inner two channels or outer two channels are labelled CI and CO, respectively. Air channels not used would not be present when the element is built and replaced by insulation. Therefore, unused air channels are simulated as insulation by assigning the corresponding material properties to the channel itself and the volume inside the unused channel. Furthermore, two application variants were investigated: heating case and cooling case. The corresponding temperature levels for the simulations are shown in Tab. 2.

Tab. 2 –Temperatures used in application variants

Study Case	Temperature		
	Room	Air inlet	Fluid inlet
Heating	20 °C	20 °C	50 °C
Cooling	26 °C	26 °C	16 °C

To establish grid-independence, a mesh refinement

study was performed for the element V03 with constant parameters. The mesh giving sufficiently accurate results considering the computational time has about 741,000 elements and a computational time of about 4.5 hours. The results of the simulation were compared with the measurement results and the required agreement of less than 15 % deviation was achieved for these investigations.

4. Results

As given in Tab. 1, 8 demonstrators were built. The numerical simulations were done with many parameters. Therefore, selected results are presented and correlations explained. Due to the limited space, only the heating case is presented. The cooling cases were equally evaluated leading to analogue results.

4.1 Experimental investigation

In the first step, the surface temperature distribution on the room-facing side of the demonstrator was analysed using thermography. Fig. 6 shows the demonstrator V03 with no air volume flow and with an air volume flow of $\dot{V}_{air}$ = 20 and 75 m³/h. It can be seen very clearly that at no and low airflow the surface temperature is higher because less heat is transferred to the air and thus more heat is transferred to the room-facing surface. Since no OCPM is installed in this demonstrator, the contact points of the pipe and sheet metal are very clearly visible in all the conditions investigated. This results in thermal hotspots on the surface.

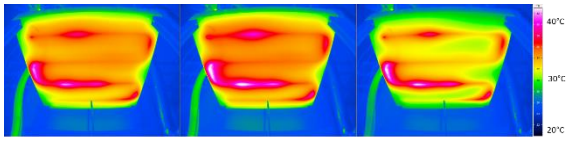

Fig. 6 – Thermography of the room-facing side demonstrator V03 at $\vartheta_{W,i}$ = 50 °C, $\dot{V}_W$ = 0.5 L/min and $\dot{V}_{air}$ = 0 m³/h (left), 20 m³/h (centre), 75 m³/h (right)

The influence of the metal foam can be seen in Fig. 7 showing demonstrator V02. The OCPM improves the heat distribution from the pipe to the room-facing surface. The thermal hotspots only occur in places at the pipe bends and are relatively smaller. Furthermore, with no or low air volume flow, a more homogeneous surface temperature distribution occurs compared to the maximum volume flow.

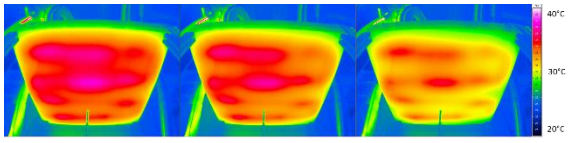

Fig. 7 – Thermography of the room-facing side demonstrator V02 at $\vartheta_{W,i}$ = 50 °C, $\dot{V}_W$ = 0.5 L/min and $\dot{V}_{air}$ = 0 m³/h (left), 20 m³/h (centre), 75 m³/h (right)

With the use of metal fibres as OCPM in demonstrator V05, a significant increase in surface temperature as well as a more homogeneous distribution can be achieved, see Fig. 8. This is caused by the better heat conduction properties of the metal fibres compared to the metal foam.

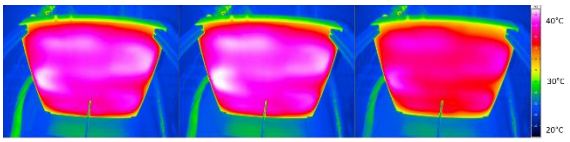

Fig. 8 – Thermography of the room-facing side demonstrator V05 $\vartheta_{W,i}$ = 50 °C, $\dot{V}_W$ = 0.5 L/min and $\dot{V}_{air}$ = 0 m³/h (left), 20 m³/h (centre), 75 m³/h (right)

The fact that the manufacturing quality has a very high influence on the thermal properties of the hybrid element can be seen in Fig. 9. The surface temperature is significantly higher and more homogeneously distributed compared to demonstrator V03 in Fig. 6.

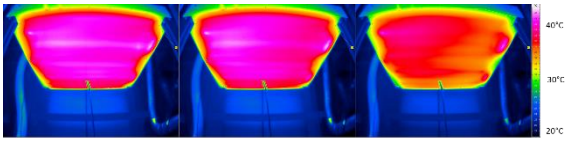

Fig. 9 – Thermography of the room-facing side demonstrator V07 at $\vartheta_{W,i}$ = 50 °C, $\dot{V}_W$ = 0.5 L/min and $\dot{V}_{air}$ = 0 m³/h (left), 20 m³/h (centre), 75 m³/h (right)

Fig. 10 shows a comparison of the heat flow emitted by the water $\dot{Q}_W$ for all demonstrators as a function of the air flow rate $\dot{V}_{air}$. All demonstrators tend to behave quite similarly - the increase in air flow rate provides an increased heat flux, which is given off by the water. The reference case V03 lies approximately in the middle of all demonstrators.

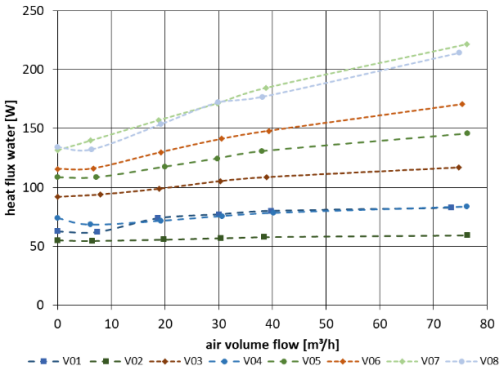

Fig. 10 – Course of the heat flux water $\dot{Q}_W$ in comparison of all demonstrators at ϑ_{Wi} = 50 °C, $\dot{V}_W$ = 0.5 L/min

The demonstrators below have either the metal foam as the OCPM (V01, V02) or the pipe lies on the OCPM metal fibres (V04). Here it can be seen that the metal foam worsens the heat transport due to its properties (e.g. thin webs, relatively large air content) and that with an unfavourable arrangement of the OCPM and tube, the OCPM acts as an additional thermal resistance. This has a clear effect on the performance of the demonstrator. In demonstrator V05, the tube is placed inside OCPM metal fibres and therefore has much better thermal contact. This is also reflected in the performance curve. Again, better

thermal properties of the hybrid element can be achieved with a higher manufacturing quality, see demonstrators V06, V07 and V08.

Regarding the heat flux density on the room-facing surface, the same statements can be made. The demonstrators with the OCPM metal foam and the demonstrator with the tubes on the OCPM metal fibres have significantly lower specific heat flux densities (Fig. 11). Comparing the heat flux densities to the reference element V03, the specific heat flux density on the room-facing surface without air volume flow can be increased to values of $\dot{q}_{room}$ = 120 ... 130 W/m² (V07, V08). It can also be seen that the drop in heat flux density of the elements V05, V07, V08 at the highest air volume flow rate is still at the level of the heat flux density of the reference element V03 without air volume flow rate. This means that despite a high air volume flow and the associated heat absorption of the air, the hybrid element can achieve a high value for the function as surface heating.

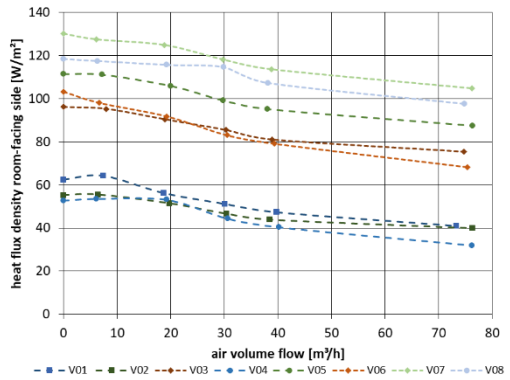

Fig. 11 – Course of the heat flux density on the room-facing side $\dot{q}_{room}$ in comparison of all demonstrators at $\vartheta_{W,i} = 50$ °C, $\dot{V}_W = 0.5$ L/min

Fig. 12 shows the change in air temperature as a function of the air flow rate for all demonstrators. Also from this point of view, the demonstrators behave as described above. With the demonstrators V06 to V08, changes in the air temperature as a function of the air volume flow of $\Delta\vartheta_{air} = 7.5$ ... 11 K are possible under the present boundary conditions.

It should be noted that this change in air temperature occurs over the 625 mm length of the hybrid element. By connecting several elements in series or by using a longer element, higher temperature changes are possible.

The influence of the water volume flow on the thermal performance of the hybrid element is small. Due to the very good heat transfer from the water to the pipe wall, this thermal resistance is negligible compared to the other heat transfer resistances in the element. In comparison, the water inlet temperature has a significant influence on the thermal behaviour of the hybrid element. The higher it is, the greater the heat fluxes that can be transferred.

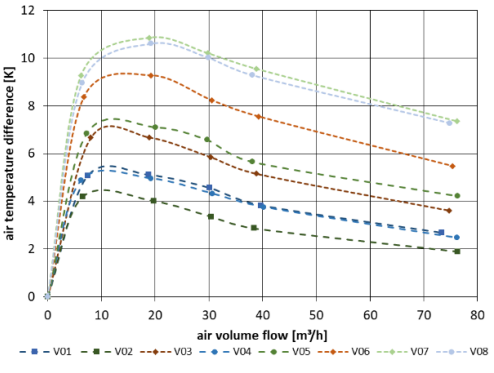

Fig. 12 – Course of air temperature difference $\Delta\vartheta_{air}$ in comparison of all demonstrators at $\vartheta_{W,VL} = 50$ °C, $\dot{V}_W = 0.5$ L/min

4.2 Numerical simulation

With all the different variations described in chapter 3.2, there are 168 parameter cases for each of the 3 geometric variants simulated. This leads to a total of 504 numerical investigated variants. For all the variants, the caloric change of the air flow and heat transfer medium was evaluated as well as the minimal, maximal and average temperatures of all surfaces. Additionally, all corresponding heat fluxes are calculated. Due to the enormous number of variants, exemplary results are discussed in the following. Presented are the results of element V03, where the differences between different variants are greatest. Subsequently, general statements and conclusions are formulated from the simulation results.

Fig. 13 shows heat flux to the air (top) $\dot{Q}_{air}$ and out of the heat transfer medium (centre) $\dot{Q}_W$ as well as the heat flux to the room (bottom) $\dot{q}_{room}$ as a function of the air flow $\dot{V}_{air}$ of element V03 with 4 air channels. The heat flux to the air and to the room are considered positive. The heat flux out of the medium is considered negative to correspond with the other heat flux directions. Note that the heat flux to the room $\dot{q}_{room}$ is given in W/m². This is to enable a simple comparison with other, commercially available systems. But the given values cannot be added according to the energy balance of the element. The left edge of the diagrams corresponds to operation as a pure radiant heating system with no air flow so no heat flux to the air is calculated. The designation of the respective curves compiles the pipe material (e.g. Cu, PE) and then the material in the tolerance range between pipe and air channel (e.g. Air, Alu). The combination "Cu/Alu" indicates a copper pipe with aluminium as gap filler in the tolerance space.

The curves show the expected pattern. As the air flow rate increases, the heat flow transferred to the air increases steadily. Thus, the corresponding temperature difference is getting smaller (not shown). The heat transfer medium shows the same behaviour, but with the opposite sign as mentioned before. The cooling of the fluid increases

continuously, as does the heat flux. This temperature change of the heat transfer fluid consequently leads to a reduced temperature of the surface facing the room, which results in a lower average excess temperature and, thus, also a lower heating output.

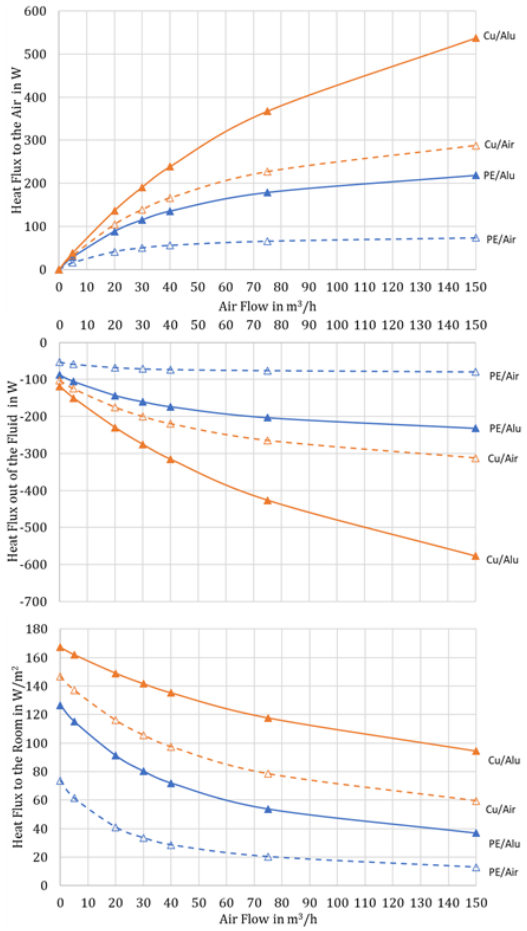

Fig. 13 – Heat flux in the air, out of the heating fluid to the room (model V03, 4 air channels, heating case)

The influence of the tolerance range between the tube and the air channel as well as the tube material is also as expected. The copper tube performs significantly better than PE tube due to the lower thermal resistance through the tube wall. If there is air between the pipe and the air channel, lower heating capacities occur as expected. Due to the direct contact between the pipe and the surfaces facing the room, the resulting differences between the tube materials are unambiguous.

This unambiguity is partially lost when OCPM is used as a heat spreader between the pipes and the surface facing the room, as considered in element V04. Fig. 14 shows the same curves for geometry variant V04. Here the variant with plastic tube and very good thermal contact (PE/Alu) approaches the combination of copper tube with air gap (Cu/Air) or performs minimally better. The combination of metallic copper pipe with ideal thermal contact is also far ahead in this case and the plastic tube with air gap performs correspondingly poorly.

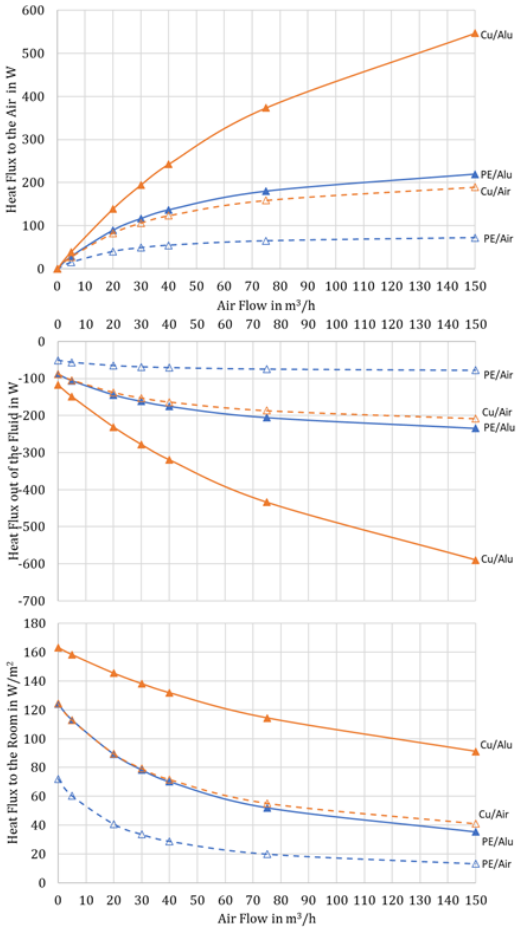

Fig. 14 – Heat flux in the air, out of the heating fluid to the room (model V04, 4 air channels, heating case)

When looking at the curves of geometry variant V05 in Fig. 15, the deviating scale values should be noted. The heating of the air and, thus, also the heat flow transferred to the air are significantly reduced. In order to achieve a clear assignment of the curves and to increase the readability of the diagrams, the axes have been adjusted. The same applies to the heat transfer fluid. However, the scaling of the axes for mean excess temperature and heat flow of the surface facing the room is unchanged.

In comparison, all 3 variants show comparable values regarding the average excess temperature of the surface facing the room and the possible heat flux. The differences in the internal structure are not visible in this illustration, but they do influence the temperature distribution and the minimum and maximum temperatures that occur.

Fig. 16 shows the temperature spread of the room facing surface for geometry variant V03 (top) and V05 (bottom) for the combination of copper pipe with air as filler. The curves show the minimum, average and maximum temperatures of the surface. In this case, when OCPM is omitted (V03), the maximum surface temperature is approximately equal to the fluid temperature. This maximum temperature is found around the inlet of the heat carrier fluid. There is a line contact between the tube and the casing sheet. Because of the air gap, the air

channel is not able to distribute the heat to the casing sheet so that the minimum surface temperature is only slightly above the room temperature. This results in spreads of up to 27 K, i.e. overheated and cold areas are formed.

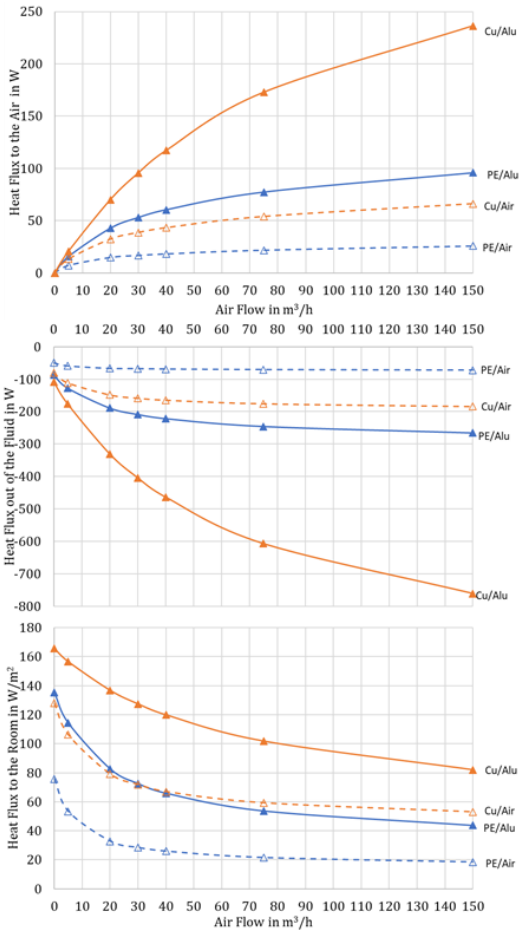

Fig. 15 – Heat flux in the air, out of the heating fluid to the room (model V05, 4 air channels, heating case)

If OCPM is installed (V05), the average surface temperatures drop by up to approximately 5 K due to the additional thermal resistance, but the spread between minimum and maximum temperature at the surface is halved to approximately 13 K.

From this it can be concluded that the use of an open-cell porous metal results in a significantly more uniform surface temperature, particularly in the case of high manufacturing tolerances, whereby the reduction in the area-specific heating power can be neglected. The previous explanations always refer to the case where all existing air channels are in use. However, it is possible to use only two air channels These can be located at the outer edge (labelled CO) or in the centre of the module (labelled CI). Fig. 17 shows the heat flux out of the heating fluid with different pipe materials and tolerance materials for model V03. The heat flux out of the fluid is lower with the same air volume flow with only two active air channels. The position of the air channels is not relevant. Corresponding results are shown by all other investigated geometries.

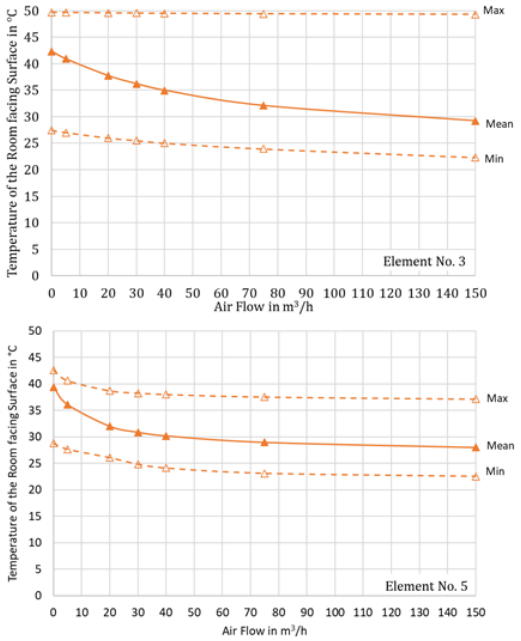

Fig. 16 – Minimum, average and maximum temperature of the room facing surface for model V03 (top) and V05 (bottom) (copper tube, air filled gap)

Identical evaluations were done for the cooling case. The signs of temperature differences and the heat fluxes are reversed. This time the fluid absorbs heat and its temperature rises. The air releases heat accordingly and cools down. The excess temperature of the room facing surface is also negative, as temperatures below the room temperature must be realised to cool the room. With this in mind, identical statements can be made about the tendencies of the temperatures and heat fluxes.

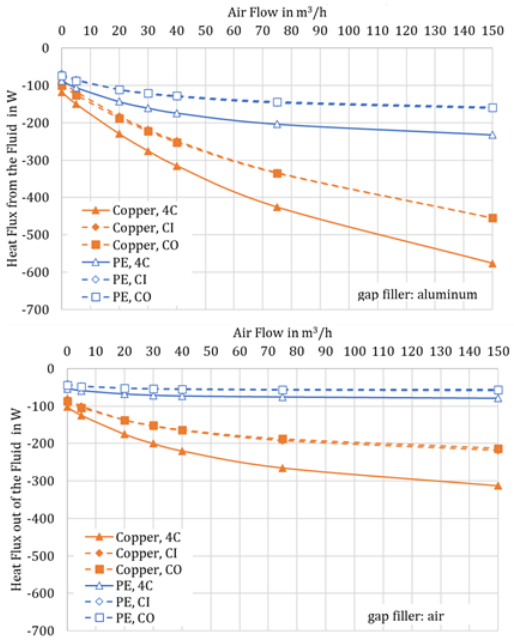

Fig. 17 – Heat flux from the heat transfer fluid for model V03

Also in the cooling case, good contact between the tube and the air channel is important for the performance of the system. The Cu/Alu case is therefore to be preferred in the cooling case. The

same applies to the comparisons between the geometry variants.

5. Conclusions

The study presented consists of experimental and extending numerical investigations. The geometrical models were comprehensively analysed and compared in terms of their thermal and energetic behaviour in heating. The given results for the heating case equally apply to the cooling case. As a result, the intended functional principle of implementing a surface heating/cooling with simultaneous conditioning of an air volume flow could be proven. Furthermore, influencing parameters on the thermal performance such as air volume flow, water volume flow and flow temperature of the water were worked out. The results of the experimental investigations under the given boundary conditions show that in the heating case an area-specific heating capacity of $\dot{q}_{room} = 130$ W/m^2 at the room facing surface can be achieved with a heating fluid of $\vartheta_{W,i} = 50$ °C. The same hybrid element extracts up to $\dot{q}_{room} = 30$ W/m^2 from the room with a fluid temperature of $\vartheta_{W,i} = 16$ °C in the cooling case. Depending on the design of the demonstrator, heat flux densities of up to $\dot{q}_{air} = 500$ W/m^2 can be transferred to the air at maximum air flow rate which results to a temperature increase of the air between $\Delta\vartheta_{air} = 7.5$ K … 11 K. Regarding the planned modes of operation, the potential control range can be defined on the basis of the course of the heat flux density to the air. The simulations carried out provided detailed findings on the influence of the thermal contact resistances between the tube and the surrounding OCPM or air channel. It is imperative to avoid high manufacturing tolerances to avoid unnecessary thermal resistances to the overall system. A very well-connected PE pipe achieves similar performance values as a copper tube with an air gap caused by manufacturing tolerances. Therefore, a lighter plastic pipe can be used if the heat transfer pipe is very well contacted. Using an OCPM reduces the possible surface temperatures by approximately $\Delta T = 5$ K, but forms a much more uniform temperature field where the spread between minimum and maximum surface temperature is reduced from $\Delta\vartheta_{SF} = 27$ K to only $\Delta\vartheta_{SF} = 13$ K in extreme cases. The heat transferred to the air flow is directly dependent on the number of active air channels, thus the position of the air channels inside the demonstrator is not relevant. The scalability of the element, the control and system integration into the building, the interaction with the user and an extensive field test are seen as the next steps.

6. Acknowledgement

This research was supported by the German Federal Ministry for Economic Affairs and Energy under the project number 03ET1512A-D

7. References

[1] Causone F., Baldin F., Olesen B. W., Corgnati S. P. Floor heating and cooling combined with displacement ventilation: Possibilities and limitations. Energy and Buildings. 2010;(42):2338-2352

[2] Riffat S. B., Zhao X., Doherty P. S. Review of research into and application of chilled ceilings and displacement ventilation systems in europe. International Journal of Energy Research. 2004;(28):257-286

[3] Khan Y., Khare V. R., Mathur J., Bhandari M. Performance evaluation of radiant cooling system integrated with air system under different operational strategies. Energy and Buildings. 2015;(97):118-128

[4] Hao X., Zhang G., Chen Y., Zou S., Moschandreas D. J. A combined system of chilled ceiling, displacement ventilation and desiccant dehumidification. Building and Environment. 2007;(42):3298-3308

[5] Andersen O., Kostmann C., Stephani G., Korb G. Application-related properties of sintered metallic fiber structures. MetFoam. 2003;481-486

[6] Fink M., Andersen O., Seidel T., Schlott A. Strongly orthotropic open cell porous metal structures for heat transfer applications. Metals. 2018;8(7):554

[7] Zhao C.Y. Review on thermal transport in high porosity cellular metal foams with open cells. Int. J. Heat Mass Tansf. 2012;55(13-14):3618-3631

[8] Veyhl C., Fiedler T., Andersen O., Meinert J., Bernthaler T., Belova I. V., Murch G. E. On the thermal conductivity of sintered metallic fibre structures. Int. J. Heat Mass Transf. 2012;55(9-10):2440-2448

[9] Schinke L., Schlott A., Beyer M., Seifert J., Fink M. Investigations on a hybrid element with cellular metallic material for heating, cooling and ventilation. E3S Web of Conferences 111, 01095 (2019), DOI:10.1051/e3sconf/201911101095.

[10] Glück, B. „Heizen und Kühlen mit Niedrigexergie (LowEx), Abschlussbericht, FKZ 0327370B," Westsächsische Hochschule Zwickau, Zwickau, 2008.

Data Statement

The datasets generated and analysed during the current study are not available because patent protection law votes are currently being carried out but the authors will make every reasonable effort to publish them in near future.